



Article

A Laboratory Approach to Measure Enhanced Gas Recovery from a Tight Gas Reservoir during Supercritical Carbon Dioxide Injection

Rahmad Syah ¹, Seyed Mehdi Alizadeh ², Karina Shamilyevna Nurgalieva ³, John William Grimaldo Guerrero ⁴, Mahyuddin K. M. Nasution ^{5,*}, Afshin Davarpanah ⁶, Dadan Ramdan ¹ and Ahmed Sayed M. Metwally ^{7,*}

- ¹ Data Science & Computational Intelligence Research Group, Universitas Medan Area, Medan 20112, Indonesia; rahmadsyah@staff.uma.ac.id (R.S.); dadan@uma.ac.id (D.R.)
- ² Petroleum Engineering Department, Australian College of Kuwait, West Mishref 13015, Kuwait; s.alizadeh@ack.edu.kw
- ³ Department of Development and Operation of Oil and Gas Fields, Saint-Petersburg Mining University, 199106 St. Petersburg, Russia; khaibullina_k@mail.ru
- ⁴ Department of Energy, Universidad de la Costa, Barranquilla 080001, Colombia; jgrimald1@cuc.edu.co
- ⁵ Data Science & Computational Intelligence Research Group, Universitas Sumatera Utara, Medan 20222, Indonesia
- ⁶ Chemistry of Interfaces, Luleå University of Technology, SE-97187 Luleå, Sweden; afshindpe@gmail.com
- ⁷ Department of Mathematics, College of Science, King Saud University, Riyadh 11451, Saudi Arabia
- * Correspondence: mahyuddin@usu.ac.id (M.K.M.N.); dalsayed@ksu.edu.sa (A.S.M.M.)



Citation: Syah, R.; Alizadeh, S.M.; Nurgalieva, K.S.; Grimaldo Guerrero, J.W.; Nasution, M.K.M.; Davarpanah, A.; Ramdan, D.; Metwally, A.S.M. A Laboratory Approach to Measure Enhanced Gas Recovery from a Tight Gas Reservoir during Supercritical Carbon Dioxide Injection. *Sustainability* **2021**, *13*, 11606. <https://doi.org/10.3390/su132111606>

Academic Editor: Fatemeh Kamali

Received: 13 September 2021

Accepted: 13 October 2021

Published: 20 October 2021

Publisher's Note: MDPI stays neutral with regard to jurisdictional claims in published maps and institutional affiliations.



Copyright: © 2021 by the authors. Licensee MDPI, Basel, Switzerland. This article is an open access article distributed under the terms and conditions of the Creative Commons Attribution (CC BY) license (<https://creativecommons.org/licenses/by/4.0/>).

Abstract: Supercritical carbon dioxide injection in tight reservoirs is an efficient and prominent enhanced gas recovery method, as it can be more mobilized in low-permeable reservoirs due to its molecular size. This paper aimed to perform a set of laboratory experiments to evaluate the impacts of permeability and water saturation on enhanced gas recovery, carbon dioxide storage capacity, and carbon dioxide content during supercritical carbon dioxide injection. It is observed that supercritical carbon dioxide provides a higher gas recovery increase after the gas depletion drive mechanism is carried out in low permeable core samples. This corresponds to the feasible mobilization of the supercritical carbon dioxide phase through smaller pores. The maximum gas recovery increase for core samples with 0.1 mD is about 22.5%, while gas recovery increase has lower values with the increase in permeability. It is about 19.8%, 15.3%, 12.1%, and 10.9% for core samples with 0.22, 0.36, 0.54, and 0.78 mD permeability, respectively. Moreover, higher water saturations would be a crucial factor in the gas recovery enhancement, especially in the final pore volume injection, as it can increase the supercritical carbon dioxide dissolving in water, leading to more displacement efficiency. The minimum carbon dioxide storage for 0.1 mD core samples is about 50%, while it is about 38% for tight core samples with the permeability of 0.78 mD. By decreasing water saturation from 0.65 to 0.15, less volume of supercritical carbon dioxide is involved in water, and therefore, carbon dioxide storage capacity increases. This is indicative of a proper gas displacement front in lower water saturation and higher gas recovery factor. The findings of this study can help for a better understanding of the gas production mechanism and crucial parameters that affect gas recovery from tight reservoirs.

Keywords: displacement efficiency; natural gas recovery; permeability; water saturation; adsorption density

1. Introduction

The enormous demand of various industries for fossil fuels [1–9] has forced petroleum industries to find novel solutions to improve the oil production rate [10–16]. Utilization of underground stored natural gas would be more environmentally friendly during enhanced recovery processes [17–23], as it does not need to transfer gas from petrochemical industries [24–26]. Moreover, it is more economical, as it has removed unprecedented expenses to capture carbon dioxide [27–34]. Recently, due to the high productions of hydrocarbon, most of the conventional reservoirs are almost depleted, or it is not economical

to produce the remained hydrocarbon [35–40]. Thereby, to provide the supply and demand for different industries, new methods such as drilling horizontal wells, hydraulic fracturing, and enhancing the production rate from unconventional reservoirs become more important [41–45]. Unconventional reservoirs include shale reservoirs, tight ($k < 10$ mD) or ultra-tight ($0.1 < k < 1$ mD) reservoirs [46–50]. Due to tight gas reservoirs' low permeability and poor reservoir characteristics [51–55], ultimate gas recovery is very low, which is not beneficial for petroleum industries [56–61]. Various studies have been conducted on the gas recovery enhancement from tight gas reservoirs; however, there is no significant progress made, compared with conventional gas reservoirs [62–67]. Problems such as liquid injection difficulties for chemical enhanced recovery methods or mixture problems of injected gas with in situ gas have caused lower displacement efficiency [68–73]. Vo Thanh et al. (2020) investigated the optimal WAG (alternating water gas) performances by a robust optimization workflow as an artificial intelligence optimizer in carbon dioxide sequestration processes for sandstone reservoirs. They illustrated that WAG injection could help to reduce the solubility trapping and residual features of carbon dioxide [74]. AlRassas et al. (2021) developed a 3D geological model to estimate the carbon dioxide capacity in the Shahejie Formation, which can be a crucial factor in determining the required carbon dioxide during injectivity processes [75]. An artificial neural network model improves this issue in offshore Vietnam, as developed by Vo Thanh et al. (2020) [76].

Although regarding the poor reservoir characteristics of tight reservoirs, gas recovery is not high enough (in the range of 35–45%), it would be the optimum choice to produce natural gas instead of conventional reservoirs, as most of the hydrocarbons are depleted [77–79]. Furthermore, chemical-based recovery methods are not feasible in tight gas reservoirs due to the liquid injection difficulties [80–86]. Carbon dioxide injection would be the more practical method, as it can be easily mixed with the formation of in situ natural gas [75,76]. The gas recovery enhancement has been improved from areas with poor displacements [87–90]. Carbon dioxide can also be stored in underground formations during the gas recovery enhancement, which is why it is called an environmentally friendly and economical method. The CO₂ phase has been changed in temperatures more than 31.04 °C and pressures more than 7.382 MPa, with different viscosity and density [91–93]. This property would be more conducive for efficient displacement in tight reservoirs. Liu et al. (2013) observed that supercritical CO₂ injection could provide more gas recovery factors in shale reservoirs—above 95% of the injected CO₂ was stored [94]. In this paper, we experimentally investigated the effect of permeability and water saturation during supercritical CO₂ injection, and how they impact the gas recovery in tight reservoirs. This process is schematically shown in Figure 1.

The prominent influence of carbon dioxide-based enhanced oil recovery methods has been studied to enhance the recovery factor in tight oil reservoirs [95–99]. Based on several studies, carbon dioxide is stored in underground formations and helps to enhance oil recovery [100–102]. Hu et al. (2020) experimentally investigated the effect of carbon dioxide injection in shale core samples for different cycles and how it affects the oil recovery factor. An increase in the number of cycles would be a potentially influential factor in enhancing the oil recovery factor. Carbon dioxide changes to the supercritical phase in higher temperatures and pressures, which causes more carbon dioxide adsorption. Higher adsorption of carbon dioxide can improve the displacement efficiency, and more oil volumes are therefore produced [103]. Yang et al. (2017) observed that it was not the natural gas features but the physical characteristics of supercritical carbon dioxide, such as viscosity and density, that caused proper displacement efficiency. Therefore, in this study, regarding these efficient features, supercritical carbon dioxide injection would be a prominent option to increase remained natural gas production from tight reservoirs [104]. Furthermore, the higher adsorption capacity of supercritical carbon dioxide, compared with natural gas (CH₄, C₂H₆, and CO₂), would be another influential factor in improving gas recovery from tight reservoirs [104–107]. According to Kim et al. (2017), gas recovery increase for a shale reservoir would be 24% more than regular carbon dioxide injection. This

paper aimed to investigate tight gas reservoirs and tight core samples during supercritical injection and examine whether lower permeabilities can provide better gas recoveries [108].

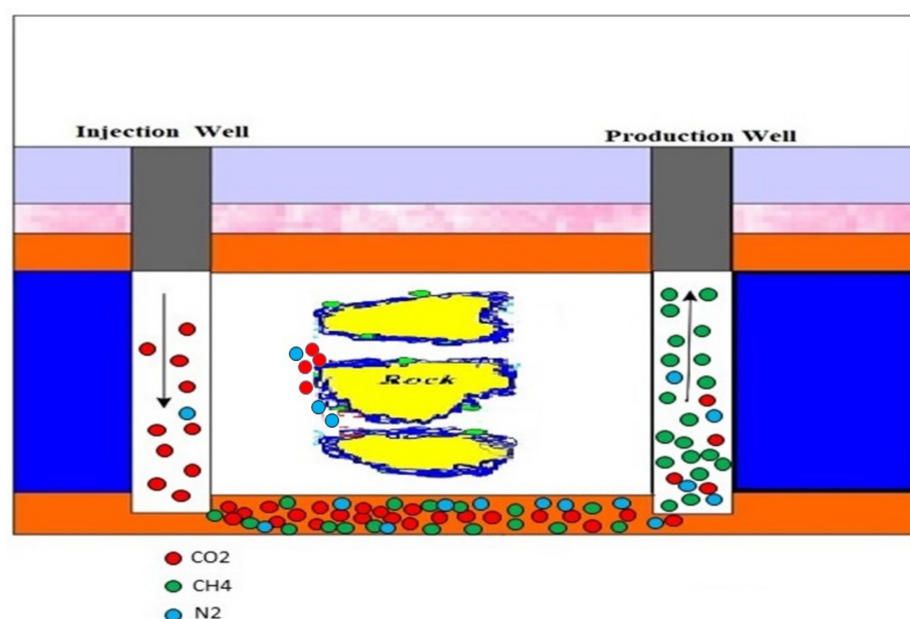


Figure 1. The supercritical CO₂ injection process through porous media. As can be seen, natural gas included CO₂, CH₄, and N₂ injected into the formation and in the production well, mostly CH₄ was produced, and CO₂ was stored for further processing.

This paper aimed to experimentally investigate the considerable influence of supercritical carbon dioxide injection for various permeabilities and water saturations in tight gas core samples to observe the gas recovery alterations. It is observed that this method is an appropriate method to improve natural gas recovery and carbon dioxide storage in lower permeable core samples. First, materials used for this experiment and their properties are introduced, and then the presented methods are explained in Section 2. Then, in Section 3, the effect of crucial parameters on enhanced gas recovery and CO₂ storage are reported and explained in more detail. Finally, the main conclusions of this study are summarized in Section 4.

2. Materials and Methods

2.1. Materials

Core samples: A total of 25 tight core samples from a gas reservoir with the permeability and porosity range of 0.05–0.9 mD and 4.23–9.49%, respectively, were selected for this experiment. The lengths are 2.5 inches and 1.5 inches, and 94% of the selected core samples contained quartz, and 6% contained calcite and dolomite. To provide a reasonable evaluation of reservoir conditions, the temperature was considered to be 60 °C.

Fluids: natural gas with 96.7% CH₄, 3% of C₃–C₅, 0.3% of N₂, and 99.9% purified CO₂, were used in the experiment. Synthetic brine with 52,000 mg·L^{−1} of KCl was used to match with formation brine.

2.2. Experimental Apparatus

The following procedure was performed to measure gas recovery for different water saturation and core permeabilities to observe their significant impact on the carbon dioxide storage and content (see Table 1). It is schematically depicted in Figure 2.

2.3. Measurement of Supercritical Carbon Dioxide Characteristics

Firstly, diffusion capacity was measured by an HTHP vessel by injecting supercritical carbon dioxide (yellow dye) in constant pressure, and then the natural gas was injected sequentially. Two gases were combined for two days under 60 °C. The measured compo-

sition and pressure drop rate were utilized to measure diffusion capacity (see Figure 3). It is observed that lower pressures have larger diffusivity in natural gas, which is about 12×10^{-8} for 10 MPa. The pressure increase decreases it.

Table 1. Supercritical carbon dioxide procedure for enhanced gas recovery.

Step	Process
1	Irreducible water with a saturation of 30% was injected into the core holder system. A pressure drop transmitter was put above the core holder to regulate the pressure if necessary.
2	Core samples were saturated with natural gas to reach the pore pressure to 25 MPa (reservoir pressure). The confining pressure was 30 MPa.
3	The gas depletion drive mechanism was started from one end of the core sample to measure the gas volume by a gas meter until it reached a plateau.
4	Supercritical carbon dioxide injection with the pressure of 12 MPa was started until all of the natural gas components were produced.

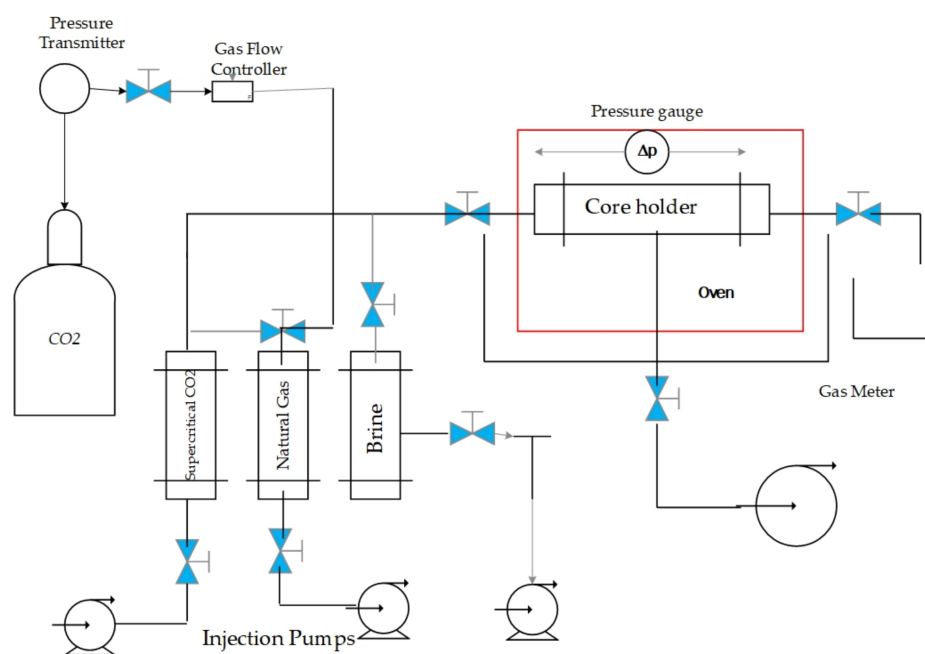


Figure 2. Supercritical carbon dioxide setup.

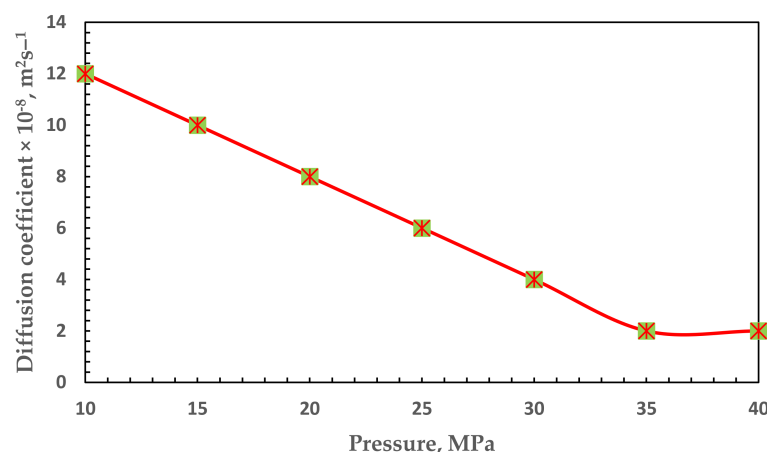


Figure 3. Diffusion coefficient at various pressures. The measured composition and pressure drop rate were utilized to measure diffusion capacity.

In this part, the thermophysical characteristics of viscosity, adsorption, and density were measured in lab conditions at different pressures (see Table 2). It is observed that supercritical carbon dioxide has a higher density and viscosity at higher temperatures, which significantly influences the gas recovery from tight reservoirs. These values are higher than natural gas viscosity and density due to the differences in gravity between supercritical carbon dioxide and natural gas. On the other hand, increased adsorption capacity by increasing pressure results in higher values for supercritical carbon dioxide than natural gas. Therefore, adsorption differentiations would be crucial in gas recovery enhancement by replacing the natural gas phase in a porous medium.

Table 2. Fluid thermophysical characteristics for supercritical carbon dioxide.

Pressure, MPa	Viscosity, mPa·s	Density, g·cm ⁻³	Adsorption Volume, cm ³ ·g ⁻¹
10	0.02	0.2	0.1
15	0.03	0.3	0.121429
20	0.04	0.4	0.142858
25	0.05	0.5	0.164287
30	0.06	0.6	0.185716
35	0.07	0.7	0.207145
40	0.08	0.8	0.228574

3. Results and Discussion

3.1. Enhanced Gas Recovery

When measuring the gas recovery from tight core samples, the results indicate that the maximum gas recovery is 46.4%, which means there is no significant progress in gas recovery. At this stage, the supercritical gas injection started to inject supercritical carbon dioxide through tight core samples. Different crucial factors such as permeability and water saturation were considered to measure the ultimate gas recovery factor. Moreover, the gas recovery increase by using supercritical carbon dioxide was measured for each factor to compare the effect of each parameter.

3.1.1. Effect of Permeability

To observe the significant impact of different permeability on the gas recovery enhancement, five different permeabilities of 0.1, 0.22, 0.36, 0.54, and 0.78 mD were considered. It is observed that supercritical carbon dioxide provides a higher gas recovery increase after the gas depletion drive mechanism is carried out in lower permeability core samples. This increase is related to the feasible mobilization of the supercritical carbon dioxide phase through smaller pores. The maximum gas recovery increase for core samples with 0.1 mD is about 22.5%, while gas recovery increase has lower values with the increase in permeability. It is about 19.8%, 15.3%, 12.1%, and 10.9% for core samples with 0.22, 0.36, 0.54, and 0.78 mD, respectively (see Figure 4).

3.1.2. Effect of Water Saturation

To consider the effect of water saturation on the gas recovery from tight reservoirs, we set water saturation levels at 0.15, 0.35, 0.45, 0.55, and 0.65 in our experiments. As shown in Figure 5, higher water saturation is a crucial factor in the gas recovery enhancement, especially in the final pore volume injection, as it can increase the supercritical carbon dioxide dissolving in water, leading to more displacement efficiency.

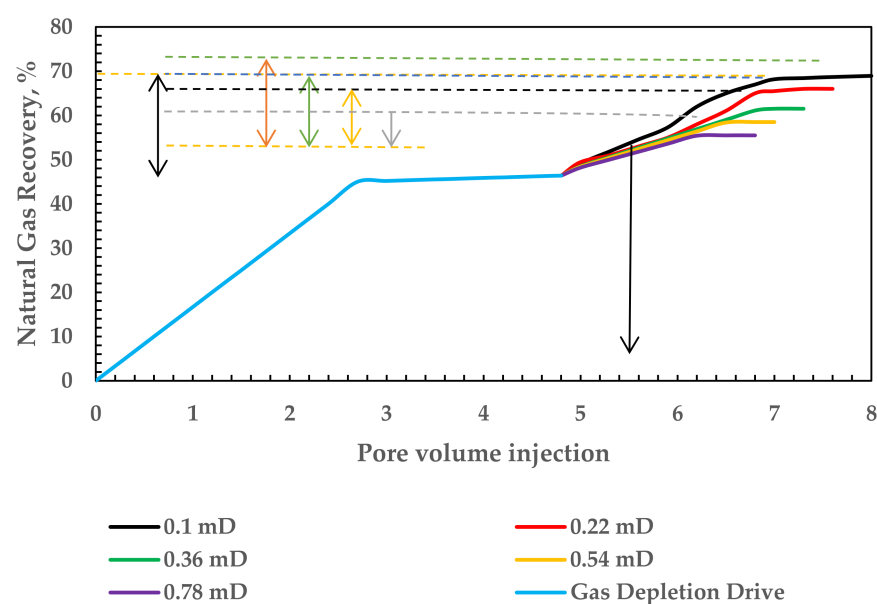


Figure 4. Effect of permeability on the gas recovery enhancement using supercritical carbon dioxide for five different permeabilities of 0.1, 0.22, 0.36, 0.54, and 0.78 mD.

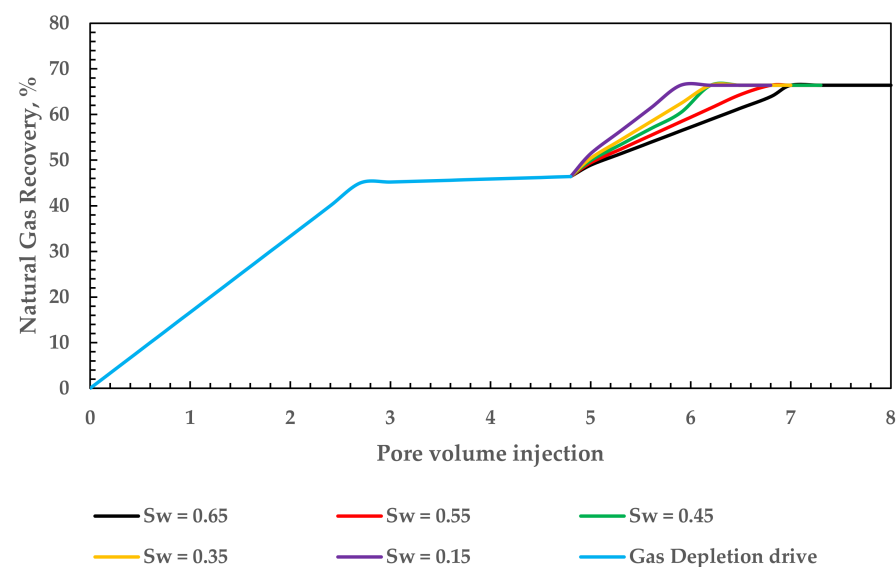


Figure 5. Effect of water saturation on the gas recovery enhancement for supercritical carbon dioxide for water saturation levels of 0.15, 0.35, 0.45, 0.55, and 0.65 in our experiments.

3.2. Carbon Dioxide Content

In the first period of supercritical carbon dioxide injection through tight core samples, there is no carbon dioxide in the produced gas. After the carbon dioxide breaks through in the pores, carbon dioxide content is increased. It becomes the only gas component in the pores, and there is no natural gas in the system. This is why the natural gas recovery from the tight core samples reaches a plateau after a short time of carbon dioxide breakthrough [109]. Another reason is the extremely low diffusivity index of supercritical carbon dioxide when in contact with natural gas.

3.2.1. Effect of Permeability

To observe the significant impact of different permeabilities on the carbon dioxide content, five different permeabilities of 0.1, 0.22, 0.36, 0.54, and 0.78 mD were considered. As shown in Figure 6, the breakthrough time is delayed by reducing core samples' permeability

during supercritical carbon dioxide injection. It causes the carbon dioxide content to increase dramatically in a shorter time. Furthermore, due to more small pores in lower permeable pores in tight core samples, natural gas would be trapped in the pores, as the gas mobilization is poor. Supercritical carbon dioxide injection can push the trapped natural gas into small pores due to being a more feasible outcome and the smaller molecular size. Another reason for this issue corresponded to the higher adsorption capacity of supercritical carbon dioxide in lower permeabilities.

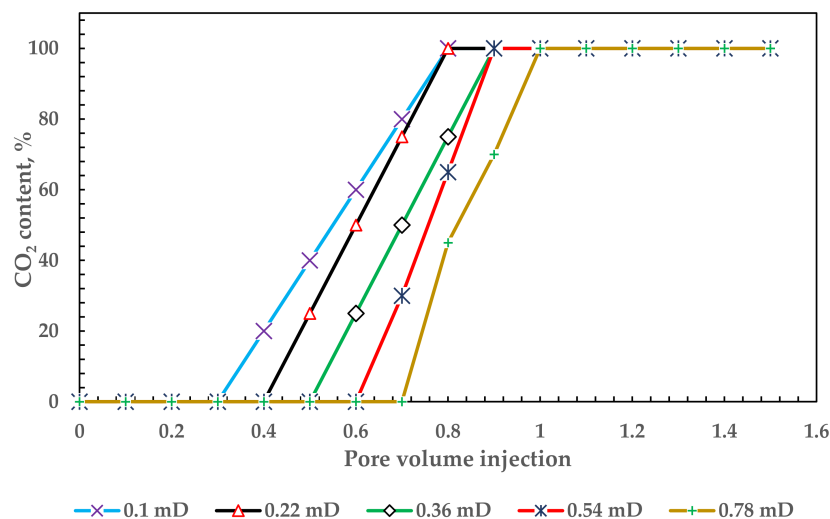


Figure 6. Effect of permeability on the carbon dioxide content in supercritical carbon dioxide injection for five different permeabilities of 0.1, 0.22, 0.36, 0.54, and 0.78 mD.

3.2.2. Effect of Water Saturation

To consider the effect of water saturation on the carbon dioxide content in supercritical carbon dioxide injection from tight reservoirs, we set water saturation levels at 0.15, 0.35, 0.45, 0.55, and 0.65 in our experiments. An increase in water saturation causes a delay in reaching the breakthrough. This corresponds to the supercritical carbon dioxide dissolving in water, which causes a proper displacement front and more gas recovery factor (see Figure 7).

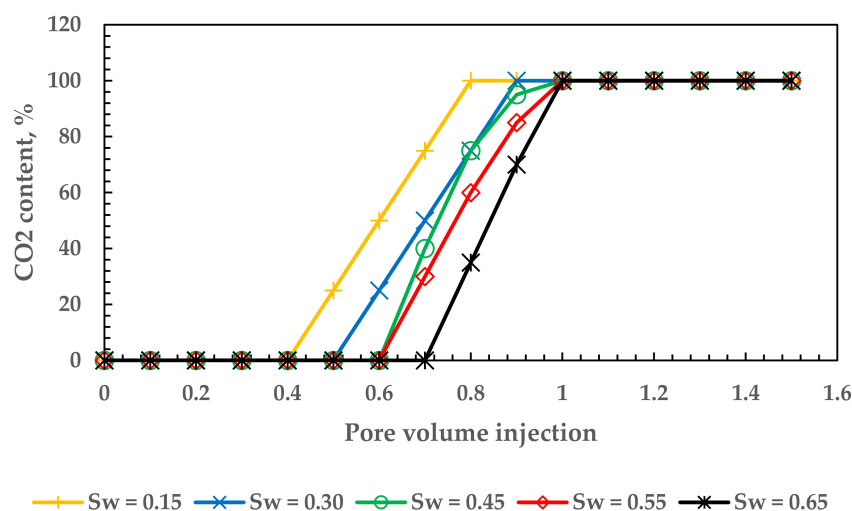


Figure 7. Effect of water saturation on the carbon dioxide content in supercritical carbon dioxide injection for water saturation levels of 0.15, 0.35, 0.45, 0.55, and 0.65 in our experiments.

3.3. Carbon Dioxide Storage Capacity

The storage capacity for carbon dioxide is defined as the storage volume to the total carbon dioxide injection volume. Before the breakthrough, there is no production of carbon

dioxide, and a large volume of carbon dioxide is stored, while after the breakthrough, its storage decreases dramatically.

3.3.1. Effect of Permeability

To observe the significant impact of different permeabilities on the carbon dioxide storage capacity, five different permeabilities of 0.1, 0.22, 0.36, 0.54, and 0.78 mD were considered. As shown in Figure 8, the carbon dioxide storage capacity decreases with the increase in core samples' permeability during supercritical carbon dioxide injection. This is due to the stronger adsorption capacity of supercritical carbon dioxide in low-permeable core samples. Therefore, it causes tight core samples to have a lower gas recovery factor. The minimum carbon dioxide storage for 0.1 mD core samples is about 50%, while it is about 38% for tight core samples with the permeability of 0.78 mD.

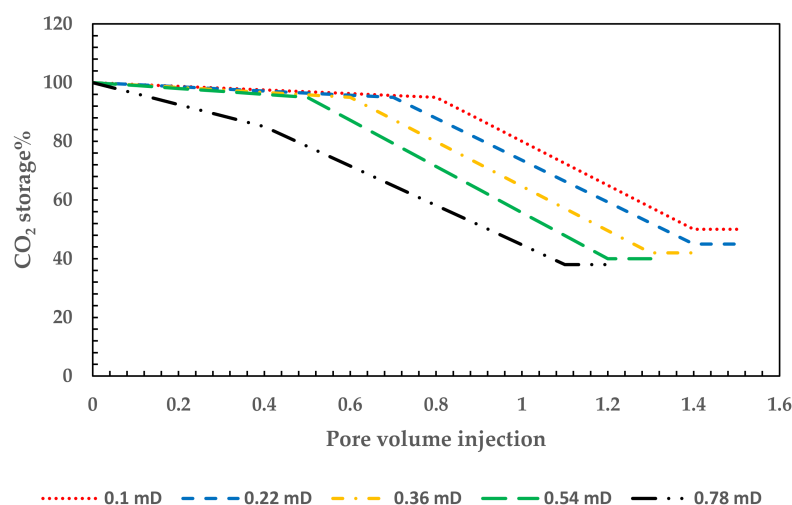


Figure 8. Effect of permeability on the carbon dioxide storage capacity in supercritical carbon dioxide injection for five different permeabilities of 0.1, 0.22, 0.36, 0.54, and 0.78 mD.

3.3.2. Effect of Water Saturation

To consider the effect of water saturation on the carbon dioxide storage capacity in supercritical carbon dioxide injection from tight reservoirs, we set water saturation levels at 0.15, 0.35, 0.45, 0.55, and 0.65 in our experiments. By decreasing water saturation from 0.65 to 0.15, less volume of supercritical carbon dioxide is involved in water, and therefore, carbon dioxide storage capacity increases. This indicates a proper gas displacement front in lower water saturation and higher gas recovery factor (see Figure 9).

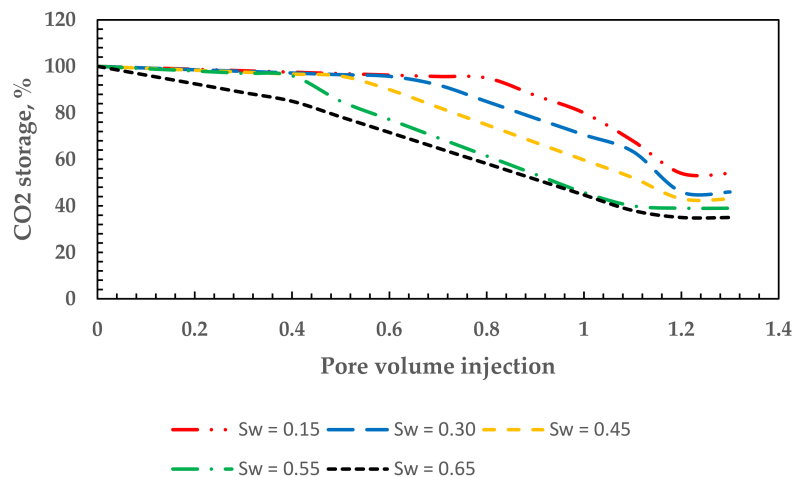


Figure 9. Effect of water saturation on the carbon dioxide storage capacity in supercritical carbon dioxide injection for water saturation levels of 0.15, 0.35, 0.45, 0.55, and 0.65 in our experiments.

3.4. Summary of Results

The results summary is depicted in Tables 3 and 4 for the effects of permeability and water saturation.

Table 3. Summary of results (effect of permeability).

Permeability	0.1 mD	0.22 mD	0.36 mD	0.54 mD	0.78 mD
Natural gas recovery increase	20%	20%	20%	20%	20%
Carbon dioxide breakthrough	0.30 PV	0.40 PV	0.50 PV	0.60 PV	0.70 PV
Carbon dioxide storage capacity at the end of 1.3 PV injection	50%	45%	42%	40%	38%

Table 4. Summary of results (effect of water saturation).

Water Saturation	0.15	0.35	0.45	0.55	0.65
Natural gas recovery increase	22.5%	19.8%	15.3%	12.1%	10.9%
Carbon dioxide breakthrough	0.4 PV	0.5 PV	0.55 PV	0.6 PV	0.7 PV
Carbon dioxide storage capacity	48%	44%	41%	39%	35%

4. Summary and Conclusions

- ✓ The maximum gas recovery increase for core samples with 0.1 mD is about 22.5%, while gas recovery increase has lower values with the increase in permeability. It is about 19.8%, 15.3%, 12.1%, and 10.9% for core samples with 0.22, 0.36, 0.54, and 0.78 mD, respectively.
- ✓ By reducing core samples' permeability during supercritical carbon dioxide injection, the breakthrough time is delayed. It causes the carbon dioxide content to increase dramatically in a shorter time.
- ✓ The carbon dioxide storage capacity is decreased by increasing core samples' permeability during supercritical carbon dioxide injection. This decrease in higher permeabilities corresponds to the more negligible adsorption of supercritical carbon dioxide.
- ✓ The minimum carbon dioxide storage for 0.1 mD core samples is about 50%, while it is about 38% for tight core samples with the permeability of 0.78 mD.
- ✓ By decreasing water saturation from 0.65 to 0.15, less volume of supercritical carbon dioxide is involved in water, and therefore, carbon dioxide storage capacity increases. This indicates a proper gas displacement front in lower water saturation and higher gas recovery factor.

Author Contributions: Conceptualization, A.D. and S.M.A.; methodology, A.D.; software, R.S.; validation, K.S.N., J.W.G.G. and A.D.; formal analysis, M.K.M.N.; investigation, A.D.; resources, D.R.; data curation, R.S.; writing—original draft preparation, S.M.A.; writing—review and editing, A.D.; visualization, A.S.M.M.; supervision, A.D.; project administration, M.K.M.N.; funding acquisition, A.S.M.M. All authors have read and agreed to the published version of the manuscript.

Funding: This work was funded by the Researchers Supporting Project No.(RSP-2021/363), King Saud University, Riyadh, Saudi Arabia.

Institutional Review Board Statement: Not applicable.

Informed Consent Statement: Not applicable.

Data Availability Statement: Not applicable.

Conflicts of Interest: The authors declare no conflict of interest.

Nomenclature

EGR	Enhanced gas recovery
EOR	Enhanced oil recovery
mD	Darcy ($\times 10^{-3}$)
CO ₂	Carbon Dioxide
CH ₄	Methane
C ₂ H ₆	Ethane
C ₃	Propane
C ₆	Hexane
N ₂	Nitrogen
KCL	Potassium chloride
S _w	Water Saturation

References

- Jassim, T.L. The Influence of Oil Prices, Licensing and Production on the Economic Development: An Empirical Investigation of Iraq Economy. *AgBioForum* **2021**, *23*, 1–11.
- Esan, B.; Hassan, A. Nexus between Carbon Dioxide Emission, Energy Consumption and Economic Growth in Nigeria. *Int. J. Sustain. Energy Environ. Res.* **2020**, *9*, 46–55. [\[CrossRef\]](#)
- Adle, A.A.; Akdemir, Ö. Achieving competitive advantage in technology based industry: How developing intellectual capital matters. *Int. J. Ebus. Govern. Stud.* **2019**, *11*, 89–103. [\[CrossRef\]](#)
- Li, A.; Mu, X.; Zhao, X.; Xu, J.; Khayatnezhad, M.; Lalehzari, R. Developing the non-dimensional framework for water distribution formulation to evaluate sprinkler irrigation. *Irrig. Drain.* **2021**, *70*, 659–667. [\[CrossRef\]](#)
- Zhou, Z.; Qin, J.; Xiang, X.; Tan, Y.; Liu, Q.; Xiong, N.N. News Text Topic Clustering Optimized Method Based on TF-IDF Algorithm on Spark. *Comput. Mater. Contin.* **2020**, *62*, 217–231. [\[CrossRef\]](#)
- Tian, L.; Li, J.; Zhang, L.; Sun, Y.; Yang, S. TCPW BR: A Wireless Congestion Control Scheme Base on RTT. *Comput. Mater. Contin.* **2020**, *62*, 233–244. [\[CrossRef\]](#)
- Syah, R.; Alizadeh, S.M.; Nasution, M.K.; Kashkouli, M.N.I.; Elveny, M.; Khan, A. Carbon dioxide-based enhanced oil recovery methods to evaluate tight oil reservoirs productivity: A laboratory perspective coupled with geo-sequestration feature. *Energy Rep.* **2021**, *7*, 4697–4704. [\[CrossRef\]](#)
- Xu, Z.; Liang, W.; Li, K.C.; Xu, J.; Jin, H. A blockchain-based roadside unit-assisted authentication and key agreement protocol for internet of vehicles. *J. Parallel Distrib. Comput.* **2021**, *149*, 29–39. [\[CrossRef\]](#)
- Wang, W.; Yang, Y.; Li, J.; Hu, Y.; Luo, Y.; Wang, X. Woodland labeling in chenzhou, China, via deep learning approach. *Int. J. Comput. Intell. Syst.* **2020**, *13*, 1393–1403. [\[CrossRef\]](#)
- Duan, Y.; Liu, Y.; Chen, Z.; Liu, D.; Yu, E.; Zhang, X.; Fu, H.; Fu, J.; Zhang, J.; Du, H. Amorphous molybdenum sulfide nanocatalysts simultaneously realizing efficient upgrading of residue and synergistic synthesis of 2D MoS₂ nanosheets/carbon hierarchical structures. *Green Chem.* **2020**, *22*, 44–53. [\[CrossRef\]](#)
- He, L.; Chen, Y.; Zhao, H.; Tian, P.; Xue, Y.; Chen, L. Game-based analysis of energy-water nexus for identifying environmental impacts during Shale gas operations under stochastic input. *Sci. Total Environ.* **2018**, *627*, 1585–1601. [\[CrossRef\]](#)
- Da'le, A.B. Developing mathematical models for global solar radiation intensity estimation at Shakardara, Kabul. *Int. J. Innov. Res. Sci. Stud.* **2021**, *4*, 133–138. [\[CrossRef\]](#)
- Li, W.; Xu, H.; Li, H.; Yang, Y.; Sharma, P.K.; Wang, J.; Singh, S. Complexity and algorithms for superposed data uploading problem in networks with smart devices. *IEEE Internet Things J.* **2019**, *7*, 5882–5891. [\[CrossRef\]](#)
- Gu, K.; Jia, W.; Zhang, J. Identity-based multi-proxy signature scheme in the standard model. *Fundam. Informaticae* **2017**, *150*, 179–210. [\[CrossRef\]](#)
- Gu, K.; Wang, Y.; Wen, S. Traceable Threshold Proxy Signature. *J. Inf. Sci. Eng.* **2017**, *33*, 63–79.
- Davarpanah, A.; Mirshekari, B. Experimental Investigation and Mathematical Modeling of Gas Diffusivity by Carbon Dioxide and Methane Kinetic Adsorption. *Ind. Eng. Chem. Res.* **2019**, *58*, 12392–12400. [\[CrossRef\]](#)
- Mosbah, A.; Ali, M.A.M.; Aljubari, I.H.; Talib, Z.M.; Sherief, S.R. Migrants in the High-Tech and Engineering Sectors: An Emerging Research Area. In Proceedings of the 2018 IEEE Conference on Systems, Process and Control (ICSPC), Melaka, Malaysia, 14–15 December 2018; pp. 234–237.
- Ahmadi, R.; Sarvestani, M.R.J.; Taghavizad; Rahim, N. Evaluating Adsorption of Proline Amino Acid on the Surface of Fullerene (C₆₀) and Carbon Nanocone by Density Functional Theory. *Chem. Methodol.* **2020**, *4*, 68–79. [\[CrossRef\]](#)
- Benson, S.; Cook, P.; Anderson, J.; Bachu, S.; Nimir, H.B.; Basu, B.; Bradshaw, J.; Deguchi, G. Chapter 5: Underground geological storage. In *IPCC Special Report on Carbon Dioxide Capture and Storage*; IPCC: Geneva, Switzerland, 2005.

20. Brodny, J. Storage of carbon dioxide in liquidated mining headings of abandoned coal mines. In Proceedings of the 17th International Multidisciplinary Scientific GeoConference SGEM2017, Science and Technologies in Geology, Exploration and Mining; Stef92 Technology, Albena, Bulgaria, 29 June–5 July 2017.
21. Zhang, J.; Wu, C.; Yang, D.; Chen, Y.; Meng, X.; Xu, L.; Guo, M. HSCS: A hybrid shared cache scheduling scheme for multiprogrammed workloads. *Front. Comput. Sci.* **2018**, *12*, 1090–1104. [\[CrossRef\]](#)
22. Zhang, J.; Sun, J.; Wang, J.; Yue, X.-G. Visual object tracking based on residual network and cascaded correlation filters. *J. Ambient. Intell. Humaniz. Comput.* **2021**, *12*, 8427–8440. [\[CrossRef\]](#)
23. Ehyaei, M.A.; Ahmadi, A.; Rosen, M.A.; Davarpanah, A. Thermodynamic Optimization of a Geothermal Power Plant with a Genetic Algorithm in Two Stages. *Processes* **2020**, *8*, 1277. [\[CrossRef\]](#)
24. He, L.; Chen, Y.; Li, J. A three-level framework for balancing the tradeoffs among the energy, water, and air-emission implications within the life-cycle shale gas supply chains. *Resour. Conserv. Recycl.* **2018**, *133*, 206–228. [\[CrossRef\]](#)
25. Cheng, X.; He, L.; Lu, H.; Chen, Y.; Ren, L. Optimal water resources management and system benefit for the Marcellus shale-gas reservoir in Pennsylvania and West Virginia. *J. Hydrol.* **2016**, *540*, 412–422. [\[CrossRef\]](#)
26. Lee, B.; Lee, Y. Distinction Between Real Faces and Photos by Analysis of Face Data. *Intell. Autom. Soft Comput.* **2020**, *26*, 133–139. [\[CrossRef\]](#)
27. Ezekiel, J.; Ebigbo, A.; Adams, B.M.; Saar, M.O. Combining natural gas recovery and CO₂-based geothermal energy extraction for electric power generation. *Appl. Energy* **2020**, *269*, 115012. [\[CrossRef\]](#)
28. Sun, H.; Yao, J.; Gao, S.-H.; Fan, D.-Y.; Wang, C.-C.; Sun, Z.-X. Numerical study of CO₂ enhanced natural gas recovery and sequestration in shale gas reservoirs. *Int. J. Greenh. Gas Control.* **2013**, *19*, 406–419. [\[CrossRef\]](#)
29. Mokhtab, S.; Poe, W.A.; Mak, J.Y. Natural Gas Liquids Recovery. In *Handbook of Natural Gas Transmission and Processing*; Gulf Professional Publishing: Houston, TX, USA, 2019; pp. 361–393. [\[CrossRef\]](#)
30. Wang, J.; Ryan, D.; Szabries, M.; Jaeger, P. A Study for Using CO₂ To Enhance Natural Gas Recovery from Tight Reservoirs. *Energy Fuels* **2019**, *33*, 3821–3827. [\[CrossRef\]](#)
31. Zhou, H.; Davarpanah, A. Hybrid Chemical Enhanced Oil Recovery Techniques. *Symmetry* **2020**, *12*, 1086. [\[CrossRef\]](#)
32. Gu, K.; Jia, W.; Jiang, C. Efficient identity-based proxy signature in the standard model. *Comput. J.* **2015**, *58*, 792–807. [\[CrossRef\]](#)
33. Chen, Y.; He, L.; Li, J.; Zhang, S. Multi-criteria design of shale-gas-water supply chains and production systems towards optimal life cycle economics and greenhouse gas emissions under uncertainty. *Comput. Chem. Eng.* **2018**, *109*, 216–235. [\[CrossRef\]](#)
34. Kim, M.; Kim, J.; Shin, M. Word Embedding Based Knowledge Representation with Extracting Relationship Between Scientific Terminologies. *Intell. Autom. Soft Comput.* **2019**, *26*, 141–147. [\[CrossRef\]](#)
35. Guo, X.; Liu, J.; Dai, L.; Liu, Q.; Fang, D.; Wei, A.; Wang, J. Friction-wear failure mechanism of tubing strings used in high-pressure, high-temperature and high-yield gas wells. *Wear* **2021**, *468*, 203576. [\[CrossRef\]](#)
36. Li, Y.; Macdonald, D.D.; Yang, J.; Qiu, J.; Wang, S. Point defect model for the corrosion of steels in supercritical water: Part I, film growth kinetics. *Corros. Sci.* **2020**, *163*, 108280. [\[CrossRef\]](#)
37. Deng, J.; Chen, J.; Wang, D. Mechanism Design and Mechanical Analysis of Multi-Suction Sliding Cleaning Robot Used in Glass Curtain Wall. *Comput. Syst. Sci. Eng.* **2019**, *34*, 201–206. [\[CrossRef\]](#)
38. Zhang, D.; Chen, X.; Li, F.; Sangaiah, A.K.; Ding, X. Seam-Carved Image Tampering Detection Based on the Cooccurrence of Adjacent LBPs. *Secur. Commun. Netw.* **2020**, *2020*, 8830310. [\[CrossRef\]](#)
39. Duan, M.; Li, K.; Ouyang, A.; Win, K.N.; Li, K.; Tian, Q. EGroupNet. *ACM Trans. Multimed. Comput. Commun. Appl.* **2020**, *16*, 1–23. [\[CrossRef\]](#)
40. Zhang, J.; Yang, K.; Xiang, L.; Luo, Y.; Xiong, B.; Tang, Q. A Self-Adaptive Regression-Based Multivariate Data Compression Scheme with Error Bound in Wireless Sensor Networks. *Int. J. Distrib. Sens. Netw.* **2013**, *9*, 913497. [\[CrossRef\]](#)
41. Zhang, X.; Sun, X.; Lv, T.; Weng, L.; Chi, M.; Shi, J.; Zhang, S. Preparation of PI porous fiber membrane for recovering oil-paper insulation structure. *J. Mater. Sci. Mater. Electron.* **2020**, *31*, 13344–13351. [\[CrossRef\]](#)
42. Fan, C.; Li, H.; Qin, Q.; He, S.; Zhong, C. Geological conditions and exploration potential of shale gas reservoir in Wufeng and Longmaxi Formation of southeastern Sichuan Basin, China. *J. Pet. Sci. Eng.* **2020**, *191*, 107138. [\[CrossRef\]](#)
43. Xue, C.; You, J.; Zhang, H.; Xiong, S.; Yin, T.; Huang, Q. Capacity of myofibrillar protein to adsorb characteristic fishy-odor compounds: Effects of concentration, temperature, ionic strength, pH and yeast glucan addition. *Food Chem.* **2021**, *363*, 130304. [\[CrossRef\]](#)
44. Yang, W.; Li, K.; Li, K. A Pipeline Computing Method of SpTV for Three-Order Tensors on CPU and GPU. *ACM Trans. Knowl. Discov. Data* **2019**, *13*, 1–27. [\[CrossRef\]](#)
45. Davarpanah, A.; Shirmohammadi, R.; Mirshekari, B.; Aslani, A. Analysis of hydraulic fracturing techniques: Hybrid fuzzy approaches. *Arab. J. Geosci.* **2019**, *12*, 402. [\[CrossRef\]](#)
46. Zou, C.; Yang, Z.; He, D.; Wei, Y.; Li, J.; Jia, A.; Chen, J.; Zhao, Q.; Li, Y.; Li, J.; et al. Theory, technology and prospects of conventional and unconventional natural gas. *Pet. Explor. Dev.* **2018**, *45*, 604–618. [\[CrossRef\]](#)
47. Wang, L.; Tian, Y.; Yu, X.; Wang, C.; Yao, B.; Wang, S.; Winterfeld, P.H.; Wang, X.; Yang, Z.; Wang, Y.; et al. Advances in improved/enhanced oil recovery technologies for tight and shale reservoirs. *Fuel* **2017**, *210*, 425–445. [\[CrossRef\]](#)
48. Li, L.; Tan, J.; Wood, D.; Zhao, Z.; Becker, D.; Lyu, Q.; Shu, B.; Chen, H. A review of the current status of induced seismicity monitoring for hydraulic fracturing in unconventional tight oil and gas reservoirs. *Fuel* **2019**, *242*, 195–210. [\[CrossRef\]](#)

49. Zhou, X.; Li, K.; Yang, Z.; Xiao, G.; Li, K. Progressive Approaches for Pareto Optimal Groups Computation. *IEEE Trans. Knowl. Data Eng.* **2019**, *31*, 521–534. [\[CrossRef\]](#)
50. Davarpanah, A.; Mirshekari, B.; Behbahani, T.J.; Hemmati, M. Integrated production logging tools approach for convenient experimental individual layer permeability measurements in a multi-layered fractured reservoir. *J. Pet. Explor. Prod. Technol.* **2018**, *8*, 743–751. [\[CrossRef\]](#)
51. Gao, H.; Li, H.A. Pore structure characterization, permeability evaluation and enhanced gas recovery techniques of tight gas sandstones. *J. Nat. Gas Sci. Eng.* **2016**, *28*, 536–547. [\[CrossRef\]](#)
52. Zarebska, K.; Ceglarska-Stefańska, G. The change in effective stress associated with swelling during carbon dioxide sequestration on natural gas recovery. *Int. J. Coal Geol.* **2008**, *74*, 167–174. [\[CrossRef\]](#)
53. Liu, K.; Yu, Z.; Saeedi, A.; Esteban, L. Effects of Permeability, Heterogeneity and Gravity on Supercritical CO₂ Displacing Gas Under Reservoir Conditions. In Proceedings of the SPE Asia Pacific Enhanced Oil Recovery Conference, Kuala Lumpur, Malaysia, 11–13 August 2015.
54. Mei, J.; Li, K.; Tong, Z.; Li, Q.; Li, K. Profit Maximization for Cloud Brokers in Cloud Computing. *IEEE Trans. Parallel Distrib. Syst.* **2019**, *30*, 190–203. [\[CrossRef\]](#)
55. Tang, Q.; Yang, K.; Li, P.; Zhang, J.; Luo, Y.; Xiong, B. An energy efficient MCDS construction algorithm for wireless sensor networks. *EURASIP J. Wirel. Commun. Netw.* **2012**, *2012*, 1–15. [\[CrossRef\]](#)
56. Wei, B.; Zhang, X.; Wu, R.; Zou, P.; Gao, K.; Xu, X.; Pu, W.; Wood, C. Pore-scale monitoring of CO₂ and N₂ flooding processes in a tight formation under reservoir conditions using nuclear magnetic resonance (NMR): A case study. *Fuel* **2019**, *246*, 34–41. [\[CrossRef\]](#)
57. Tian, X.; Cheng, L.; Cao, R.; Zhang, M.; Guo, Q.; Wang, Y.; Zhang, J.; Cui, Y. Potential evaluation of CO₂ storage and enhanced oil recovery of tight oil reservoir in the Ordos Basin, China. *J. Environ. Biol.* **2015**, *36*, 789–797. [\[PubMed\]](#)
58. Orozco, D.; Fragoso, A.; Selvan, K.; Noble, G.; Aguilera, R. Eagle Ford Huff ‘n’ Puff Gas-Injection Pilot: Comparison of Reservoir-Simulation, Material Balance, and Real Performance of the Pilot Well. *SPE Reserv. Eval. Eng.* **2020**, *23*, 247–260. [\[CrossRef\]](#)
59. Esfandiyari, H.; Moghani, A.; Esmaeilzadeh, F.; Davarpanah, A. A Laboratory Approach to Measure Carbonate Rocks’ Adsorption Density by Surfactant and Polymer. *Math. Probl. Eng.* **2021**, *2021*, 5539245. [\[CrossRef\]](#)
60. Deng, Z.; Liu, C.; Zhu, Z. Inter-hours rolling scheduling of behind-the-meter storage operating systems using electricity price forecasting based on deep convolutional neural network. *Int. J. Electr. Power Energy Syst.* **2021**, *125*, 106499. [\[CrossRef\]](#)
61. Deng, Z.; Wang, B.; Xu, Y.; Xu, T.; Liu, C.; Zhu, Z. Multi-Scale Convolutional Neural Network With Time-Cognition for Multi-Step Short-Term Load Forecasting. *IEEE Access* **2019**, *7*, 88058–88071. [\[CrossRef\]](#)
62. Hamza, A.; Hussein, I.A.; Al-Marri, M.J.; Mahmoud, M.; Shawabkeh, R. Impact of clays on CO₂ adsorption and enhanced gas recovery in sandstone reservoirs. *Int. J. Greenh. Gas Control* **2021**, *106*, 103286. [\[CrossRef\]](#)
63. Teklu, T.W.; Li, X.; Zhou, Z.; Alharthy, N.; Wang, L.; Abass, H. Low-salinity water and surfactants for hydraulic fracturing and EOR of shales. *J. Pet. Sci. Eng.* **2018**, *162*, 367–377. [\[CrossRef\]](#)
64. Unconventional Gas Production from Hydraulically Fractured Well-An Application of Direct Search Based Optimization Algorithm. *Int. J. Recent Technol. Eng.* **2019**, *8*, 2726–2737. [\[CrossRef\]](#)
65. Roshani, M.; Phan, G.T.; Ali, P.J.M.; Roshani, G.H.; Hanus, R.; Duong, T.; Corniani, E.; Nazemi, E.; Kalmoun, E.M. Evaluation of flow pattern recognition and void fraction measurement in two phase flow independent of oil pipeline’s scale layer thickness. *Alex. Eng. J.* **2021**, *60*, 1955–1966. [\[CrossRef\]](#)
66. Roshani, M.; Phan, G.; Roshani, G.H.; Hanus, R.; Nazemi, B.; Corniani, E.; Nazemi, E. Combination of X-ray tube and GMDH neural network as a nondestructive and potential technique for measuring characteristics of gas-oil–water three phase flows. *Measurement* **2021**, *168*, 108427. [\[CrossRef\]](#)
67. Chen, Y.; Li, K.; Yang, W.; Xiao, G.; Xie, X.; Li, T. Performance-Aware Model for Sparse Matrix-Matrix Multiplication on the Sunway TaihuLight Supercomputer. *IEEE Trans. Parallel Distrib. Syst.* **2019**, *30*, 923–938. [\[CrossRef\]](#)
68. Jia, B.; Tsau, J.-S.; Barati, R. Role of molecular diffusion in heterogeneous, naturally fractured shale reservoirs during CO₂ huff-n-puff. *J. Pet. Sci. Eng.* **2018**, *164*, 31–42. [\[CrossRef\]](#)
69. Wang, L.; Yu, W. Gas Huff and Puff Process in Eagle Ford Shale: Recovery Mechanism Study and Optimization. In Proceedings of the SPE Oklahoma City Oil and Gas Symposium, Oklahoma City, OK, USA, 8–12 April 2019.
70. Roshani, M.; Phan, G.; Faraj, R.H.; Phan, N.-H.; Roshani, G.H.; Nazemi, B.; Corniani, E.; Nazemi, E. Proposing a gamma radiation based intelligent system for simultaneous analyzing and detecting type and amount of petroleum by-products. *Nucl. Eng. Technol.* **2021**, *53*, 1277–1283. [\[CrossRef\]](#)
71. Roshani, M.; Sattari, M.A.; Ali, P.J.M.; Roshani, G.H.; Nazemi, B.; Corniani, E.; Nazemi, E. Application of GMDH neural network technique to improve measuring precision of a simplified photon attenuation based two-phase flowmeter. *Flow Meas. Instrum.* **2020**, *75*, 101804. [\[CrossRef\]](#)
72. Karami, A.; Roshani, G.H.; Khazaei, A.; Nazemi, E.; Fallahi, M. Investigation of different sources in order to optimize the nuclear metering system of gas–oil–water annular flows. *Neural Comput. Appl.* **2018**, *32*, 3619–3631. [\[CrossRef\]](#)
73. Chen, J.; Li, K.; Bilal, K.; Zhou, X.; Li, K.; Yu, P.S. A Bi-layered Parallel Training Architecture for Large-Scale Convolutional Neural Networks. *IEEE Trans. Parallel Distrib. Syst.* **2019**, *30*, 965–976. [\[CrossRef\]](#)

74. Thanh, H.V.; Sugai, Y.; Nguele, R.; Sasaki, K. Robust optimization of CO₂ sequestration through a water alternating gas process under geological uncertainties in Cuu Long Basin, Vietnam. *J. Nat. Gas Sci. Eng.* **2020**, *76*, 103208. [\[CrossRef\]](#)
75. AlRassas, A.M.; Ren, S.; Sun, R.; Thanh, H.V.; Guan, Z. CO₂ storage capacity estimation under geological uncertainty using 3-D geological modeling of unconventional reservoir rocks in Shahejie Formation, block Nv32, China. *J. Pet. Explor. Prod. Technol.* **2021**, *11*, 2327–2345. [\[CrossRef\]](#)
76. Thanh, H.V.; Sugai, Y.; Sasaki, K. Impact of a new geological modelling method on the enhancement of the CO₂ storage assessment of E sequence of Nam Vang field, offshore Vietnam. *Energy Sources Part A Recover. Util. Environ. Eff.* **2019**, *42*, 1499–1512. [\[CrossRef\]](#)
77. Santiago, C.; Kantzas, A. Investigating the effects of gas type and operation mode in enhanced gas recovery in unconventional reservoirs. *J. Nat. Gas Sci. Eng.* **2018**, *50*, 282–292. [\[CrossRef\]](#)
78. Dai, Z.; Viswanathan, H.; Middleton, R.; Pan, F.; Ampomah, W.; Yang, C.; Jia, W.; Xiao, T.; Lee, S.-Y.; McPherson, B.; et al. CO₂ Accounting and Risk Analysis for CO₂ Sequestration at Enhanced Oil Recovery Sites. *Environ. Sci. Technol.* **2016**, *50*, 7546–7554. [\[CrossRef\]](#)
79. Song, Y.; Zhang, D.; Tang, Q.; Tang, S.; Yang, K. Local and nonlocal constraints for compressed sensing video and multi-view image recovery. *Neurocomputing* **2020**, *406*, 34–48. [\[CrossRef\]](#)
80. Pal, S.; Mushtaq, M.; Banat, F.; Al Sumaiti, A.M. Review of surfactant-assisted chemical enhanced oil recovery for carbonate reservoirs: Challenges and future perspectives. *Pet. Sci.* **2018**, *15*, 77–102. [\[CrossRef\]](#)
81. Ahmadi, M.; Chen, Z. Challenges and future of chemical assisted heavy oil recovery processes. *Adv. Colloid Interface Sci.* **2020**, *275*, 102081. [\[CrossRef\]](#)
82. Zhou, S.; Qiu, J. Enhanced SSD with interactive multi-scale attention features for object detection. *Multimed. Tools Appl.* **2021**, *80*, 11539–11556. [\[CrossRef\]](#)
83. Tang, Q.; Wang, K.; Yang, K.; Luo, Y.-S. Congestion-Balanced and Welfare-Maximized Charging Strategies for Electric Vehicles. *IEEE Trans. Parallel Distrib. Syst.* **2020**, *31*, 2882–2895. [\[CrossRef\]](#)
84. Davarpanah, A. A feasible visual investigation for associative foam polymer injectivity performances in the oil recovery enhancement. *Eur. Polym. J.* **2018**, *105*, 405–411. [\[CrossRef\]](#)
85. Davarpanah, A. Parametric Study of Polymer-Nanoparticles-Assisted Injectivity Performance for Axisymmetric Two-Phase Flow in EOR Processes. *Nanomaterials* **2020**, *10*, 1818. [\[CrossRef\]](#)
86. Kvamme, B. Feasibility of simultaneous CO₂ storage and CH₄ production from natural gas hydrate using mixtures of CO₂ and N₂. *Can. J. Chem.* **2015**, *93*, 897–905. [\[CrossRef\]](#)
87. Cranganu, C. In-situ thermal stimulation of gas hydrates. *J. Pet. Sci. Eng.* **2009**, *65*, 76–80. [\[CrossRef\]](#)
88. Yang, H.; Xu, Z.; Fan, M.; Gupta, R.; Slimane, R.B.; E Bland, A.; Wright, I. Progress in carbon dioxide separation and capture: A review. *J. Environ. Sci.* **2008**, *20*, 14–27. [\[CrossRef\]](#)
89. Song, Y.; Li, J.; Chen, X.; Zhang, D.; Tang, Q.; Yang, K. An efficient tensor completion method via truncated nuclear norm. *J. Vis. Commun. Image Represent.* **2020**, *70*, 102791. [\[CrossRef\]](#)
90. Wang, J.; Chen, W.; Ren, Y.; Alfarraj, O.; Wang, L. Blockchain based data storage mechanism in cyber physical system. *J. Internet Technol.* **2021**, *21*, 1681–1689. [\[CrossRef\]](#)
91. Wang, Z.-W.; Wang, T.-J.; Wang, Z.-W.; Jin, Y. Organic modification of nano-SiO₂ particles in supercritical CO₂. *J. Supercrit. Fluids* **2006**, *37*, 125–130. [\[CrossRef\]](#)
92. Wang, X.; Luan, Z.; Li, K.; Li, L.; Tang, T. Progress in Application of Aerogels as Adsorbents for Gas Purification. *Cailiao Daobao/Mater. Rev.* **2018**, *32*, 2214–2222. [\[CrossRef\]](#)
93. Wang, J.; Wu, W.; Liao, Z.; Jung, Y.W.; Kim, J.U. An enhanced PROMOT algorithm with D2D and robust for mobile edge computing. *J. Internet Technol.* **2020**, *21*, 1437–1445. [\[CrossRef\]](#)
94. Liu, F.; Ellett, K.; Xiao, Y.; Rupp, J.A. Assessing the feasibility of CO₂ storage in the New Albany Shale (Devonian–Mississippian) with potential enhanced gas recovery using reservoir simulation. *Int. J. Greenh. Gas Control* **2013**, *17*, 111–126. [\[CrossRef\]](#)
95. Zuloaga, P.; Yu, W.; Miao, J.; Sepehrnoori, K. Performance evaluation of CO₂ Huff-n-Puff and continuous CO₂ injection in tight oil reservoirs. *Energy* **2017**, *134*, 181–192. [\[CrossRef\]](#)
96. Huang, J.; Jin, T.; Barrufet, M.; Killough, J. Evaluation of CO₂ injection into shale gas reservoirs considering dispersed distribution of kerogen. *Appl. Energy* **2020**, *260*, 114285. [\[CrossRef\]](#)
97. Zhang, D.; Wang, S.; Li, F.; Tian, S.; Wang, J.; Ding, X.; Gong, R. An Efficient ECG Denoising Method Based on Empirical Mode Decomposition, Sample Entropy, and Improved Threshold Function. *Wirel. Commun. Mob. Comput.* **2020**, *2020*, 1–11. [\[CrossRef\]](#)
98. Mazarei, M.; Davarpanah, A.; Ebadati, A.; Mirshekari, B. The feasibility analysis of underground gas storage during an integration of improved condensate recovery processes. *J. Pet. Explor. Prod. Technol.* **2018**, *9*, 397–408. [\[CrossRef\]](#)
99. Davarpanah, A.; Mirshekari, B. Experimental study of CO₂ solubility on the oil recovery enhancement of heavy oil reservoirs. *J. Therm. Anal. Calorim.* **2020**, *139*, 1161–1169. [\[CrossRef\]](#)
100. Tang, Q.; Wang, K.; Song, Y.; Li, F.; Park, J.H. Waiting Time Minimized Charging and Discharging Strategy Based on Mobile Edge Computing Supported by Software-Defined Network. *IEEE Internet Things J.* **2020**, *7*, 6088–6101. [\[CrossRef\]](#)
101. Wang, M.; Deng, C.; Chen, H.; Wang, X.; Liu, B.; Sun, C.; Chen, G.; El-Halwagi, M.M. An analytical investigation on the energy efficiency of integration of natural gas hydrate exploitation with H₂ production (by in situ CH₄ reforming) and CO₂ sequestration. *Energy Convers. Manag.* **2020**, *216*, 112959. [\[CrossRef\]](#)

-
102. Lee, H.; Triviño, M.L.T.; Hwang, S.; Kwon, S.H.; Lee, S.G.; Moon, J.H.; Yoo, J.; Gil Seo, J. In Situ Observation of Carbon Dioxide Capture on Pseudo-Liquid Eutectic Mixture-Promoted Magnesium Oxide. *ACS Appl. Mater. Interfaces* **2018**, *10*, 2414–2422. [[CrossRef](#)]
 103. Hu, X.; Xie, J.; Cai, W.C.; Wang, R.; Davarpanah, A. Thermodynamic effects of cycling carbon dioxide injectivity in shale reservoirs. *J. Pet. Sci. Eng.* **2020**, *195*, 107717. [[CrossRef](#)]
 104. Sun, Y.; Du, Z.; Sun, L.; Pan, Y. Phase behavior of SCCO₂ sequestration and enhanced natural gas recovery. *J. Pet. Explor. Prod. Technol.* **2017**, *7*, 1085–1093. [[CrossRef](#)]
 105. Weissman, S. Diffusion Coefficients for CO₂–CH₄. *J. Chem. Phys.* **1971**, *54*, 1881–1883. [[CrossRef](#)]
 106. Davarpanah, A.; Mazarei, M.; Mirshekari, B. A simulation study to enhance the gas production rate by nitrogen replacement in the underground gas storage performance. *Energy Rep.* **2019**, *5*, 431–435. [[CrossRef](#)]
 107. Ebadati, A.; Akbari, E.; Davarpanah, A. An experimental study of alternative hot water alternating gas injection in a fractured model. *Energy Explor. Exploit.* **2018**, *37*, 945–959. [[CrossRef](#)]
 108. Kim, T.H.; Cho, J.; Lee, K.S. Evaluation of CO₂ injection in shale gas reservoirs with multi-component transport and geomechanical effects. *Appl. Energy* **2017**, *190*, 1195–1206. [[CrossRef](#)]
 109. Oldenburg, C.; Law, D.-S.; Le Gallo, Y.; White, S. Mixing of CO₂ and CH₄ in Gas Reservoirs Code Comparison Studies. In *Proceedings of the Greenhouse Gas Control Technologies—6th International Conference*, Kyoto, Japan, 1–4 October 2002; pp. 443–448.